Chinese Chemical Letters 33 (2022) 3478–3483

Contents lists available at ScienceDirect

Chinese Chemical Letters

journal homepage: www.elsevier.com/locate/cclet

Building multipurpose nano-toolkit by rationally decorating NIR-II fluorophore to meet the needs of tumor diagnosis and treatment

Chaoxiang Cui[a], Jiachen Li[a], Jing Fang[a], Yan Zhao[a], Yuqi Zhang[a], Shuyue Ye[a], Anna Wang[a], Yali Feng[a], Qiulian Mao[a], Hongni Qin[b], Haibin Shi[a,*]

[a] State Key Laboratory of Radiation Medicine and Protection, School for Radiological and Interdisciplinary Sciences (RAD-X) and Collaborative Innovation Center of Radiation Medicine of Jiangsu Higher Education Institutions, Soochow University, Suzhou 215123, China
[b] Suzhou Industrial Park Institute of Services Outsourcing, Suzhou 215123, China

ARTICLE INFO

Article history:
Received 30 January 2022
Revised 4 March 2022
Accepted 6 March 2022
Available online 9 March 2022

Keywords:
Phototheranostics
NIR-II probe
Cyanine fluorophore
Photoacoustic imaging
Photothermal therapy

ABSTRACT

Phototheranostics have attracted tremendous attention in cancer diagnosis and treatment because of the noninvasiveness and promising effectiveness. Developing advanced phototheranostic agents with long emission wavelength, excellent biocompatibility, great tumor-targeting capability, and efficient therapeutic effect is highly desirable. However, the mutual constraint between imaging and therapeutic functions usually hinders their wide applications in biomedical field. To balance this contradiction, we herein rationally designed and synthesized three novel tumor-targeted NIR-II probes (QR-2PEG$_{321}$, QR-2PEG$_{1000}$, and QR-2PEG$_{5000}$) by conjugating three different chain lengths of PEG onto an integrin $\alpha_v\beta_3$-targeted NIR-II heptamethine cyanine fluorophore, respectively. In virtue of the essential amphiphilic characteristics of PEG polymers, these probes display various degree of aggregation in aqueous buffer accompanying with differential NIR-II imaging and photothermal (PTT) therapeutic performance. Both *in vitro* and *in vivo* results have demonstrated that probe QR-2PEG$_{5000}$ has the best NIR-II imaging performance with prominent renal clearance, whereas QR-2PEG$_{321}$ possesses excellent photoacoustic signal as well as PTT effect, which undoubtedly provides a promising toolbox for tumor diagnosis and therapy. We thus envision that these synthesized probes have great potential to be explored as a toolkit for precise diagnosis and treatment of malignant tumors.

Cancer is one of the major diseases with high morbidity and mortality. Sensitive detection and efficient treatment of malignant tumors still remain a huge challenge in clinics, and have attracted wide attention from researchers [1]. Although great progress and improvement have been made in the diagnosis and treatment of tumors in past decades, there is still a long distance from the achievement of very early diagnosis and effective treatment [2–5]. Therefore, great efforts are urgently made to exploit advanced theranostic agents for battling cancers.

In contrast to traditional imaging modalities, such as magnetic resonance imaging, computed tomography, and positron emission tomography [6–11], optical imaging technology has drawn huge attention in clinical and preclinical research due to noninvasiveness, low cost, high resolution and sensitivity [12–14]. The near-infrared II (NIR-II, 900–1700 nm) fluorescence imaging especially shows great potential for *in vivo* bioimaging due to the deep tissue penetration, low fluorescence background, and superior resolution. Currently, many NIR-II fluorescent probes, such as organic small molecules [15–19], rare earth nanomaterials [20,21] conjugated polymers [22–24], carbon nanotubes [25], have been developed for visualiztion of biological events in living system. By contrast, organic small-molecule NIR-II probes essentially show a great potential for extensive applications in biomedical field owing to the excellent biocompatibility, ease of synthesis, and potential biodegradability [26–29]. Nevertheless, most of the reported NIR-II probes still encounter these dilemmas, *e.g.,* low quantum yield [30–32], poor water solubility [33–36], weak targeting capability [37,38], which severely impedes their clinical application and translation. Thus, developing novel NIR-II fluorescent probes with high stability, great biocompatibility, and good targeting capability is highly desirable for sensitive detection and efficient treatment of tumors *in vivo*.

In our previously reported work, we have successfully developed a tumor-targeting NIR-II probe QT-RGD for NIR-II/PA/SPECT multimodal imaging and photothermal therapy of tumors *in vivo*. However, its fluorescence quantum yield and water solubility need

* Corresponding author.
E-mail address: hbshi@suda.edu.cn (H. Shi).

https://doi.org/10.1016/j.cclet.2022.03.023
1001-8417/

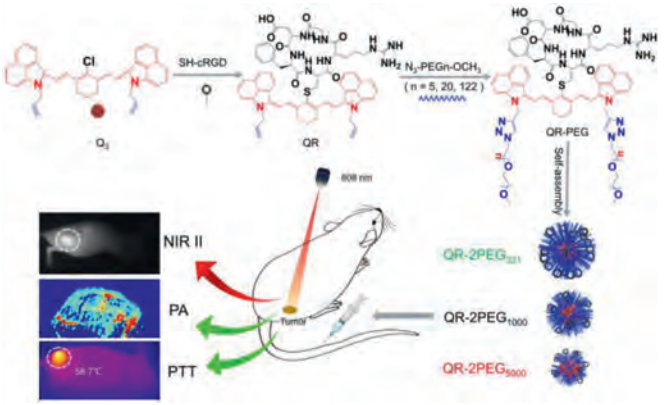

Scheme 1. Construction and applications of three novel NIR-II probes.

to be further improved so as to realize more broad application [39]. To this end, we herein rationally designed and constructed three novel theranostic probes for NIR-II/PA imaging or PTT applications of gastric tumor. As illuminated in Scheme 1, the probe consists of three components including a NIR-II heptamethine cyanine fluorophore, one $\alpha_v\beta_3$ integrin-targeted cyclic cRGD peptide for tumor targeting, and three different PEG chains with various lengths ($n = 5$, 20 and 122) attempting to improve the water solubility, biocompatibility as well as tumor delivery efficience as PEG polymer has been demonstrated to be able to effectively reduce platelet aggregation [40,41]. Due to their different amphiphilicity, these probes can self-assemble into different size of nanoparticles in aqueous buffer, showing a variety of different performance on *in vivo* tumor imaging and PTT. *In vivo* experimental results have demonstrated probe QR-2PEG$_{5000}$ has the best NIR-II imaging capability for *in vivo* gastric tumor, while QR-2PEG$_{321}$ possesses the strongest photoacoustic signal as well as PTT effect, highly indicating that these probes can potentially be used for *in vivo* tumor imaging and PTT applications.

The study started with the synthesis of the Cl-substituted heptamethine cyanine fluorophore Q_3 according to our previously reported method [39]. As illustrated in Scheme S1 (Supporting information), compound Q_3 first reacted with SH-bearing cyclic RGD peptide in DMF for 24 h to afford intermediate QR. The probe QR-2PEG$_{321}$, QR-2PEG$_{1000}$, and QR-2PEG$_{5000}$ were subsequently synthesized by "click" reaction between QR and 2 equiv. of azido-bearing PEG with different length chains ($n = 5$, 20 and 122) in DMSO and water mixture for 2 h incubation. All the intermediates and desired probes were characterized by MALDI-TOF mass spectrometry (Figs. S1–S5 in Supporting information).

The absorption spectra of three probes in organic solvents (such as DMSO, methanol) or water were first measured. As shown in Fig. 1a and Fig. S6a (Supporting information), three probes show similar absorption profile in the range of 700–1100 nm with one major absorption peak at 1045 nm. However, the probes dispersed in aqueous solution presented the maximal absorbance at 864 nm, while the peak at 1045 nm become small shoulder (Figs. S6b and c in Supporting information), which may be due to the formation of oligomers and monomers of the probes. Additionally, the absorption spectra of the probes in different proportion of DMSO and water (f_w) were measured in order to investigate the water solubility of three probes. When the water fraction increases to 100%, the absorption peak of 1045 nm dramatically increases to a maximum at 40% (f_w), and then gradually decreases to a minimum accompanying with progressive absorbance increase at 864 nm (Fig. S7 in Supporting information), implying that the probes are amphiphilic. By contrast, QR-2PEG$_{5000}$ aqueous solution exhibits the highest absorption intensity at 1045 nm, while the absorbance of QR-2PEG$_{321}$ is the lowest, suggesting that the water solubility of the probes is improved with the increase of PEG chain lengths from 321 to 5000. This can be further validated by the corresponding fluorescence spectra of three probes in organic solvent or aqueous solutions under 808 nm excitation. Fig. 1b and Fig. S8a (Supporting information) show that all three probes have very similar fluorescence spectra profile with a maximum fluorescence peak at 1065 nm in DMSO or methanol. However, QR-2PEG$_{5000}$ exhibited the strongest NIR-II fluorescence at 1065 nm compared to other two probes (Figs. S8b and c in Supporting information). Moreover, IR-26 dye was chosen as a reference (QY = 0.05%, Table S1 in Supporting information), the fluorescence quantum yields (Φ) of QR-2PEG$_{321}$, QR-2PEG$_{1000}$ and QR-2PEG$_{5000}$ were determined to be 0.03%, 0.08% and 0.17%, respectively [42]. Regarding to the blue-shift of the maximal peak position in aqueous solution, we speculate that it may be due to the water solubility difference of the probes that can be induced to form various degree of nanoaggregates. To this end, the aggregating behavior of these three probes in aqueous solution was further characterized by dynamic light scattering (DLS) analysis. The hydrodynamic diameters were determined to be 106.8 nm, 74.3 nm and 32.7 nm for QR-2PEG$_{321}$, QR-2PEG$_{1000}$, and QR-2PEG$_{5000}$ (Fig. 1c). In addition, the transmission electron microscopy (TEM) results further indicated that all three probes dispersed in aqueous solution very well as spherical nanoparticles with the sizes of 101.4 ± 0.12 nm, 66.4 ± 1.3 nm, and 27.3 ± 0.8 nm, respectively (Figs. 1d–f), which is quite close to the results of DLS analysis. Besides, no obvious size change was observed for all probes over 7 days (Figs. S9–S11 in Supporting information), suggesting that these probes have great stability in aqueous solution.

To evaluate the NIR-II imaging ability of three probes, the fluorescence images in aqueous solution were acquired with various long pass filters from 880 nm to 1250 nm. Fig. 1g shows that QR-2PEG$_{5000}$ has the significantly highest fluorescence signals than that of QR-2PEG$_{1000}$ and QR-2PEG$_{321}$ under 880, 1000, and 1150 nm, again confirming that QR-2PEG$_{5000}$ possesses a high QY yield and good water solubility. To evaluate the photostability of the probes, we carried out the standard photon-bleaching experiments for them with ICG, a clinically used NIR dye, as a reference. As shown in Fig. 1h and Fig. S12 (Supporting information), the 20 min of continuous 808 nm laser excitation only caused a little decrease of the absorption for three probes solution, while the absorption of ICG dramatically dropped within 5 min by ~95% under the same condition, implying that these three probes have outstanding photostability. Collectively, all these evidences suggest probe QR-2PEG$_{5000}$ has a high potential for *in vivo* bioimaging application.

Since the probes have strong absorption in the near-infrared regions according to the afore-mentioned results, we next determined the PA signals of three probes under 808 nm excitation. Fig. 1i clearly indicates that the PA signals of all three probes in aqueous solution gradually enhanced with the increasing concentrations. In contrast, QR-2PEG$_{321}$ has the strongest PA intensity in comparison with QR-2PEG$_{1000}$ and QR-2PEG$_{5000}$ at the same concentration, which is just the opposite of the NIR-II signals shown in Fig. 1g and Fig. S13 (Supporting information). This should be attributed to the fact that the fluorescence emitted by NIR dyes is mainly produced through the radiative transition while the PA production is mainly from non-radiative transition. Hence, fluorescence and PA are essentially a pair of competitors. Next, we evaluated the PA behavior of them. As expected, the aqueous solutions of all probes exhibited a gradually enhanced PA signal at 808 nm. The PA intensities of QR-2PEG$_{321}$ enhanced most significantly with the increase of the concentrations of the probes from 0 to 10 μmol/L, and showed a good linear relationship, indicating that QR-2PEG$_{321}$ is a promising PA imaging contrast agent.

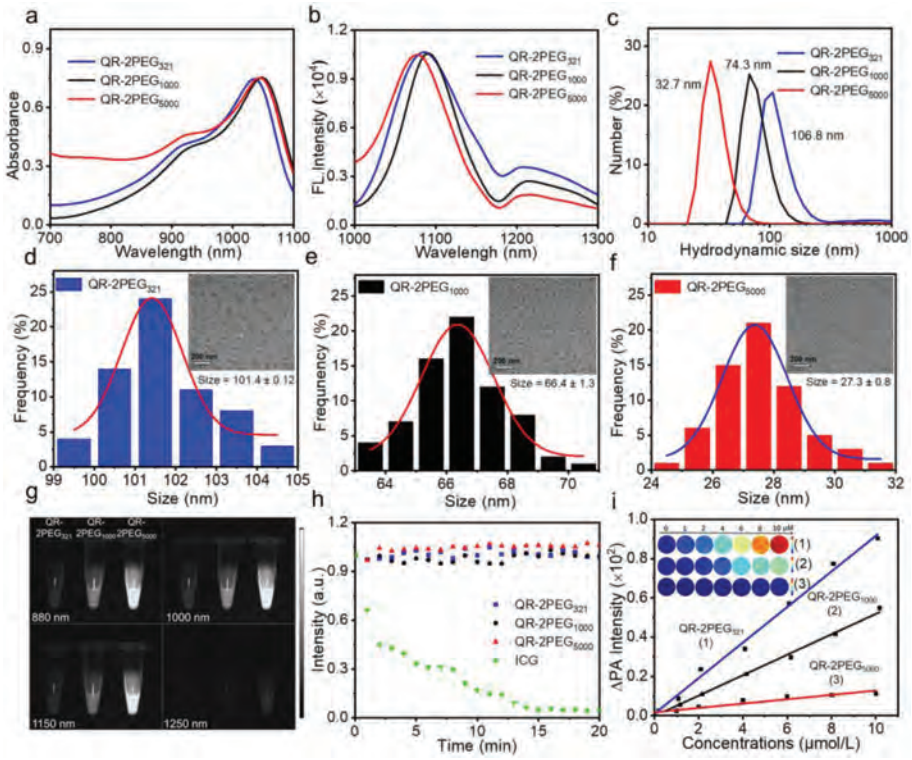

Fig. 1. Characterization and optical property of the probes. (a) Absorption and (b) fluorescence spectra of three probes QR-2PEG$_{321}$, QR-2PEG$_{1000}$, QR-2PEG$_{5000}$ (5 μmol/L) in DMSO. (c) DLS results of three probes. Size distribution profiles of QR-2PEG$_{321}$ (d), QR-2PEG$_{1000}$ (e), and QR-2PEG$_{5000}$ (f) in H_2O. The inset shows the TEM image. Scale bar: 200 nm. (g) Fluorescence images of three probes under different long-pass filters. (h) Photostabilities of the probes in aqueous solution under continuous 808 nm irradiation for 20 min. ICG was subjected to the same treatment as reference. (i) Linearity curve of ΔPA *versus* concentrations of three probes ranging from 0 to 10 μmol/L.

Encouraged by above excellent PA behavior of the probes in solution, their PTT effects were further investigated in aqueous solution. Different concentrations of QR-2PEG$_{321}$, QR-2PEG$_{1000}$ and QR-2PEG$_{5000}$ were continuously exposed to 808 nm laser (1.0 W/cm^2, 10 min). Meanwhile, the pure water was chosen as control. Their temperature change was monitored with an infrared camera. No significant temperature increase was observed for pure water, whereas various degrees of temperature increase was obviously determined for three probes with the increase of concentrations (Figs. 2a, Figs. S14a and b in Supporting information). Among them, the solution containing QR-2PEG$_{321}$ had the highest temperature raise that is up to 30.4 °C at the concentration of 16 μmol/L. However, the temperature increases of QR-2PEG$_{1000}$ and QR-2PEG$_{5000}$ is 27.2 and 22.4 °C (Fig. 2b), respectively, under the same condition, which can be also validated by the corresponding infrared (IR) thermal images (Fig. S15 in Supporting information). The photothermal conversion efficiency (η [%]) was further determined to be 43.8%, 40.3%, and 38.9% for QR-2PEG$_{321}$, QR-2PEG$_{1000}$ and QR-2PEG$_{5000}$ (Fig. 2c). In addition, the temperature increase of all three probes solution was proportional to laser power density (Fig. S16 in Supporting information). Moreover, the photothermal stability of three probes were also assessed. No significant temperature decay was monitored in 5 cycles of heating/cooling (Fig. S17 in Supporting information), suggesting that all three probes have excellent photothermal stability. Collectively, these results highly demonstrate that probe QR-2PEG$_{321}$ may be an excellent photothermal agent for PTT application, which prompts us to investigate its therapeutic efficacy against MGC-803 cells with the live/dead staining and MTT assay. Fig. 2d and Fig. S18 (Supporting information) show serious cell death was clearly detected from the cells with the treatment of QR-2PEG$_{321}$ (8 or 16 μmol/L) and 808 laser irradiation (10 min, 0.75 W/cm^2) in comparison with the ones treated with QR-2PEG$_{5000}$ and 808 laser irradiation. The MTT results further demonstrate that probe QR-2PEG$_{321}$ have obviously higher cytotoxicity to cells than QR-2PEG$_{5000}$ under the irradiation of 808 nm (Figs. 2e and f), again revealing that QR-2PEG$_{321}$ possesses prominent photothermal efficacy.

Inspired by above exciting findings, we further evaluated the performance of the probes on NIR-II/PA imaging and PTT *in vivo*. The cytotoxicity of the probes on human gastric adenocarcinoma cells MGC-803 and mouse embryonic fibroblast cells NIH/3T3 was first investigated through the standard MTT assays. All three probes showed negligible cytotoxicity towards both two types of cells below 32 μmol/L of concentration, and the overall cell viability remains above 85% after 24 h incubation, indicating they have superior biocompatibility (Fig. S19 in Supporting information), which is further supported by the red blood cell hemolysis test and blood biochemical analysis (Figs. S20 and S21 in Supporting information). Since the *in vitro* experimental results have already demonstrated that these three probes are highly NIR-II emissive, we then explored their potential for *in vivo* bioimaging. The fluorescence images of the hind limb blood vessels were first acquired in the mice with intravenous injection of probes QR-2PEG$_{321}$, QR-2PEG$_{1000}$ or QR-2PEG$_{5000}$ at 2 min. As shown in Fig. S22 (Supporting information), the deep vasculature could be clearly visualized with a high signal-to-noise contrast and super resolution under 808 nm excitation at different wavelength from 880 nm to 1150 nm for the mice receiving QR-2PEG$_{5000}$, while blurry vessels and tissues were observed for the mice with QR-2PEG$_{321}$ or QR-2PEG$_{5000}$, suggesting that QR-2PEG$_{5000}$ is more suitable for bioimaging in living system. Furthermore, the whole-body real-time fluorescence imaging of the mice with intravenous injection of probes indicates that the bladder region of the mice receiving QR-2PEG$_{5000}$ presented remarkably stronger fluorescence within 5 min than that of the mice with other two probes (Fig. 3a and Fig. S23 in Supporting information). The fluorescence signals in the bladder were gradually en-

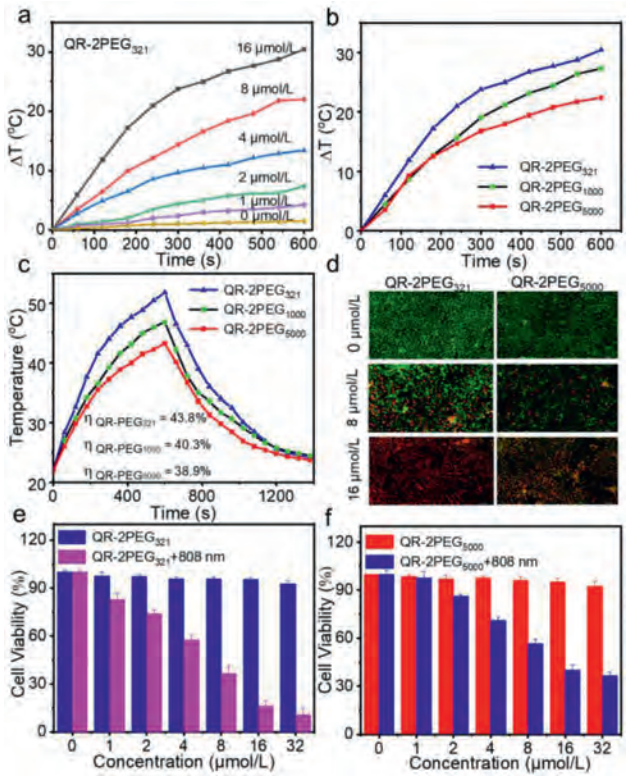

Fig. 2. Photothermal effect study of the probes. (a) Temperature variation curves of different concentrations of QR-2PEG$_{321}$ upon the irradiation of 808 nm (1 W/cm^2). (b) Heating of three probes (16 μmol/L) in aqueous solution under 808 nm irradiation. (c) Heating and cooling profiles of three probes (16 μmol/L) in aqueous solution. (d) Live/dead staining of MGC-803 cells incubated with different concentrations of QR-2PEG$_{321}$ and QR-2PEG$_{5000}$ for 24 h with the power density 0.75 W/cm^2. (e) Cytotoxicity assays of MGC-803 cells with different concentrations of QR-2PEG$_{321}$ and QR-2PEG$_{5000}$ (f) with and without 808 nm irradiation.

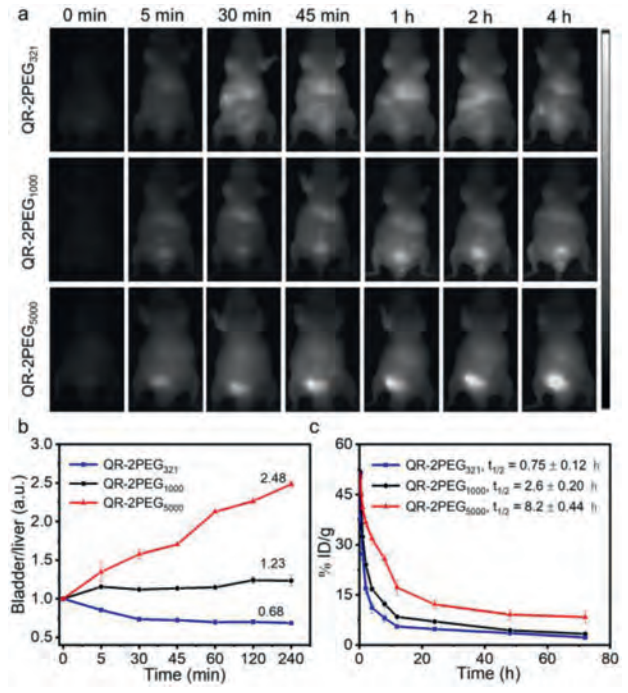

Fig. 3. The visualization of the metabolism of the probes. (a) Real-time NIR-II imaging of the mice with the intravenous injection of the probes. (b) The bladder-to-liver ratios of the fluorescence intensity from (a). (c) Blood clearance curves of three probes after intravenous injection. Error bar indicates SD ($n = 3$).

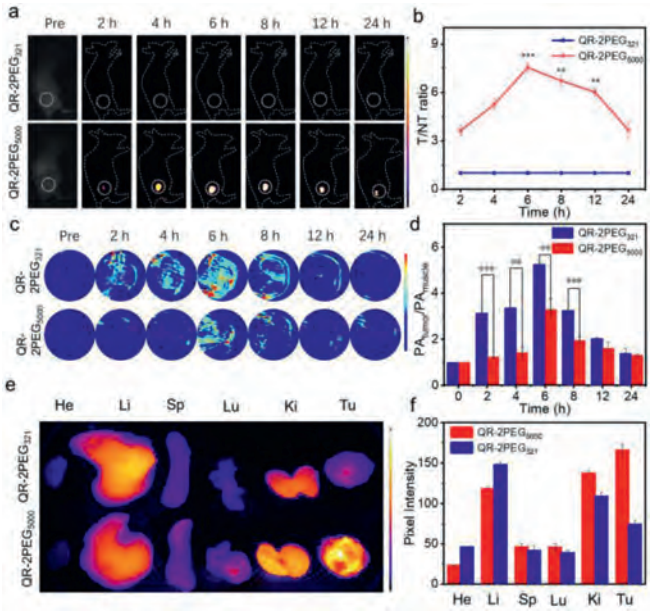

Fig. 4. NIR-II/PA imaging of MGC-803 tumors with QR-2PEG$_{321}$ and QR-2PEG$_{5000}$. (a) NIR-II images of the tumor-bearing mice at various time points post-injection of the probes (8 mg/kg). (b) The quantitative results of (a). (c) PA images of the tumor-bearing mice at different time intervals post-injection. Scale bar: 2 mm. (d) The quantitative intensity of (c). (e) The biodistribution of both probes in the tumor-bearing mice 6 h post-injection. (f) Pixel intensity of main organs and tumors ($n = 3$, $^{**}P < 0.01$, $^{***}P < 0.001$, t-test).

hanced over time, which should be because of the excellent water solubility of QR-2PEG$_{5000}$ (Fig. 3b). Next, the blood circulation dynamics of all probes was studied by monitoring their concentration in blood at different time intervals post-injection. The blood circulation half-life ($t_{1/2}$) of QR-2PEG$_{321}$, QR-2PEG$_{1000}$ and QR-2PEG$_{5000}$ is calculated to be 0.75 ± 0.12 h, 2.6 ± 0.20 h, and 8.2 ± 0.44 h (Fig. 3c), indicating that the high molecular weight of PEG chain can endow the probe with a prolonged blood circulation time. Collectively, these exciting results strongly reveal that QR-2PEG$_{5000}$ has rapid renal excretion and can be potentially applied for *in vivo* bioimaging.

To evaluate the fluorescence imaging capability of QR-2PEG$_{5000}$ for MGC-803 tumors in living mice, we performed real-time NIR-II fluorescence imaging for the tumor-bearing mice after intravenous injection of the probes (8 mg/kg). QR-2PEG$_{321}$ was chosen as a control for the same treatment. As shown in Fig. 4a, the MGC-803 tumors receiving QR-2PEG$_{5000}$ could be clearly imaged, and the fluorescence intensity of the tumor region reached a maximum 6 h post-injection with a signal-to-background ratio (SBR) of 7.4, while weak fluorescence was detected from the tumors receiving QR-2PEG$_{321}$ (SBR ≈ 1.0) (Fig. 4b). Meanwhile, the real-time PA imaging of tumors was also performed. As shown in Figs. 4c and d, the PA signals at tumor site were enhanced significantly with the time increasing, and reached the maximum at 6 h after injection, while the tumors receiving QR-2PEG$_{5000}$ exhibited much low PA signals. The SBR of PA (PA_{tumor}/PA_{muscle}) was quantified to be 5.25 and 3.28 for them. These results again demonstrate that QR-2PEG$_{5000}$ has excellent NIR-II fluorescence capability but QR-2PEG$_{321}$ emits intensive PA signals. To investigate the *in vivo* biodistribution of these two probes, the tumor and main organs including heart, liver, spleen, lung and kidneys were resected at 6 h post-injection of probes and collected for *ex vivo* fluorescence imaging. Figs. 4e and f indicate that the probes mainly distributed in liver, kidneys, and tumor of the mice. As expected, the fluorescence of the tumor with QR-2PEG$_{5000}$ is significantly stronger than that of the tumor receiving QR-2PEG$_{321}$. Together, these evidences well demon-

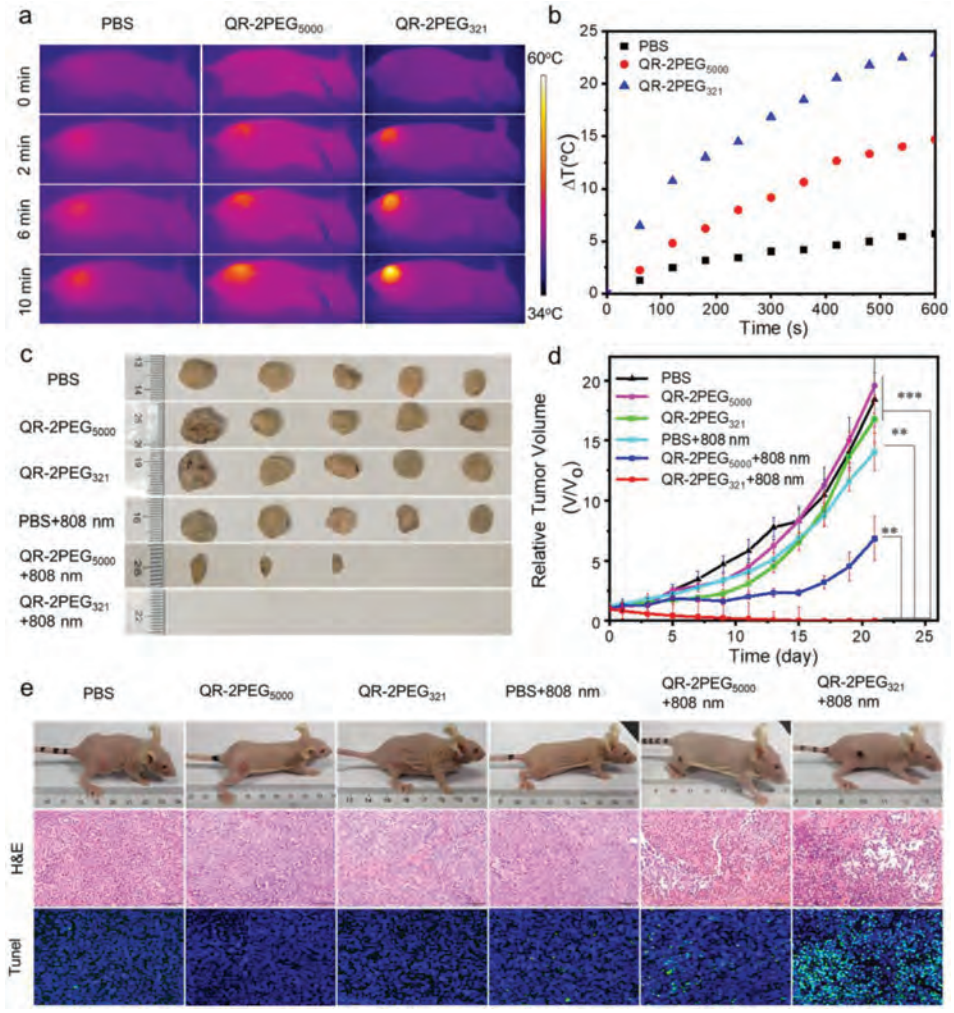

Fig. 5. *In vivo* PTT of gastric tumors. (a) Real-time infrared thermal images of MGC-803 tumor-bearing mice under 808 nm irradiation (1 W/cm^2) after intravenous injection of PBS, QR-2PEG$_{321}$ and QR-2PEG$_{5000}$ (8 mg/kg). (b) Temperature increase of (a). (c) Images of gastric tumors resected from different treatment groups ($n = 5$). (d) Relative tumor volumes in different treatment groups. (e) Images, H&E and tunnel test staining of the tumor sections of representative mice on the 3rd day post-treatment ($n = 5$, $^{**}P < 0.01$, $^{***}P < 0.001$, *t*-test).

strate that probe QR-2PEG$_{5000}$ has a great potential for *in vivo* NIR-II imaging of tumors.

The prominent PTT effect of probe QR-2PEG$_{321}$ *in vitro* prompted us to explore its feasibility in photothermal therapy of tumors. The MGC-803-bearing mice were intravenously injected with QR-2PEG$_{321}$ and QR-2PEG$_{5000}$ (8 mg/kg), respectively, through the tail vein, and the tumors were subsequently irradiated by 808 nm laser (1 W/cm^2, 10 min) at 6 h post injection. The tumors receiving QR-2PEG$_{321}$ showed obvious temperature increase up to 22.9 °C, while the QR-2PEG$_{5000}$ or PBS treated groups have only 14.6 and 5.68 °C of temperature increase under the same condition (Figs. 5a and b). To further assess the *in vivo* photothermal ablation effect of the probes, the MGC-803 tumor-bearing mice (~20 mm^3) were divided into six groups ($n = 5$) for different combination treatments. The PTT efficacy of each group was validated by monitoring the sizes of tumors over 21 days. Fig. 5c shows the size of tumors in PBS, PBS+808 nm, QR-2PEG$_{321}$, and QR-2PEG$_{5000}$ groups increases in a rather similar manner, whereas the tumor growth was inhibited in a certain degree for the QR-2PEG$_{5000}$+808 nm group. In sharp contrast, the tumors in the QR-2PEG$_{321}$+808 nm group showed a significant reduction in size upon the irradiation of 808 nm laser. Eventually, all tumors in five groups were eliminated completely (Fig. 5d and Fig. S24 in Supporting information). The survival rate curve indicates that the mice of QR-2PEG$_{321}$+808 nm have a great survival rate without even single death after 36 days (Fig. S25 in Supporting information). Moreover, we resected, sliced the tumors on day 3 post-treatment, and the tissues were then subjected to hematoxylin and eosin (H&E) staining as well as tunnel test. As show in Fig. 5e, severe necrosis and karyopyknosis were detected in QR-2PEG$_{321}$+808 nm group. However, almost no necrosis was determined in other control groups. Furthermore, the H&E staining images of the main organs collected from the mice in experimental group indicated that no obvious damage and liver metastasis were detected in comparison with the control groups (Fig. S26 in Supporting information). Besides, all groups of mice did not loss body weight during 21 days of treatment (Fig. S27 in Supporting information). Collectively, all these evidences highly demonstrate probe QR-2PEG$_{321}$ would be a promising agent for effective PTT of malignant human gastric adenocarcinoma.

In summary, we has successfully developed three novel NIR-II probes by conjugating three different chain lengths of PEG onto an integrin $\alpha_v\beta_3$-targeted NIR-II fluorophore for tumor imaging and therapy. Due to various amphipathic nature, these probes could form uniform nanoparticles with various sizes in aqueous solution showing differential NIR-II imaging and PA/PTT performance. A lot of results have demonstrated that probe QR-2PEG$_{5000}$ has outstanding capability for NIR-II imaging applica-

tion with quick renal clearance. However, QR-2PEG$_{321}$ possesses effective photoacoustic and PTT effect, which undoubtedly provides a useful toolbox for tumor theranostics. We thus envision that these synthesized probes could be exploited as a universal toolkit for achieving precise diagnosis and treatment of malignant tumors.

Declaration of competing interest

The authors declare that they have no known competing financial interests or personal relationships that could have appeared to influence the work reported in this paper.

Acknowledgments

We acknowledge financial support from the Training Program of the Major Research Plan of the National Natural Science Foundation of China (No. 91959123), National Natural Science Foundation of China (No. 22077092), Key Research and Development Program of Social Development of Jiangsu Province (No. BE2018655), the Open Project Program of the State Key Laboratory of Radiation Medicine and Protection (Nos. GZK1202132, GZK1202140 and GZK1202017), and a project funded by the Priority Academic Program Development of Jiangsu Higher Education Institutions.

Supplementary materials

Supplementary material associated with this article can be found, in the online version, at doi:10.1016/j.cclet.2022.03.023.

References

[1] A. Patel, V.G. Gupta, Lancet Oncol. 19 (2018) e328.
[2] K.K. Turaga, L.K. Kvols, CA Cancer J. Clin. 61 (2011) 113–132.
[3] J. He, C. Li, L. Ding, et al., Adv. Mater. 31 (2019) 1902409.
[4] O. Elemento, C. Leslie, J. Lundin, et al., Nat. Rev. Cancer 21 (2021) 747–752.
[5] J. Tseng, J. Miller, X. Feng, et al., J. Clin. Oncol. 39 (2021) 174.
[6] H.J. Kim, A.Y. Kim, S.T. Oh, et al., Radiology 236 (2005) 879–885.
[7] M.J. Leveridge, P.J. Bostrom, G. Koulouris, et al., Nat. Rev. Urol. 7 (2010) 311–325.
[8] Y.H. Kim, Y.J. Lee, J.H. Park, et al., Radiology 267 (2013) 414–421.
[9] T. Hayes, E. Smyth, A. Riddell, et al., Hematol. Oncol. Clin. North Am. 31 (2017) 427–440.
[10] T. Heye, R. Knoerl, T. Wehrle, et al., Radiology 295 (2020) 593–605.
[11] J. Duell, F. Krummenast, A. Schirbel, et al., J. Nucl. Med. 62 (2021) 1415–1421.
[12] A.J. Wilson, D. Devasia, P.K. Jain, Chem. Soc. Rev. 49 (2020) 6087–6112.
[13] Y. Jiang, K. Pu, Chem. Rev. 121 (2021) 13086–13131.
[14] X. Fan, Y. Li, Z. Feng, et al., Adv. Sci. 8 (2021) 2003972.
[15] S. Zhu, Z. Hu, R. Tian, et al., Adv. Mater. 30 (2018) 1802546.
[16] S. Zhu, R. Tian, A.L. Antaris, et al., Adv. Mater. 31 (2019) e1900321.
[17] J. Li, Y. Liu, Y. Xu, et al., Coord. Chem. Rev. 415 (2020) 213318.
[18] S. Wang, B. Li, F. Zhang, ACS Cent. Sci. 6 (2020) 1302–1316.
[19] Q. Wang, B. Xia, J. Xu, et al., Mater. Chem. Front. 3 (2019) 650–655.
[20] M. Zhang, W. Zheng, Y. Liu, et al., Angew. Chem. Int. Ed. 58 (2019) 9556–9560.
[21] H. Li, X. Wang, X. Li, et al., Chem. Mater. 32 (2020) 3365–3375.
[22] B. Ding, Y. Xiao, H. Zhou, et al., J. Med. Chem. 62 (2019) 2049–2059.
[23] Y. Yang, X. Fan, L. Li, et al., ACS Nano 14 (2020) 2509–2521.
[24] T. Li, C. Li, Z. Ruan, et al., ACS Nano 13 (2019) 3691–3702.
[25] Z.A. De los Santos, Z. Lin, M. Zheng, J. Am. Chem. Soc. 143 (2021) 20628–20632.
[26] C. Li, Q. Wang, ACS Nano 12 (2018) 9654–9659.
[27] Y. Suo, F. Wu, P. Xu, et al., Adv. Healthc. Mater. 8 (2019) e1900974.
[28] C. Li, G. Chen, Y. Zhang, et al., J. Am. Chem. Soc. 142 (2020) 14789–14804.
[29] Y. Zhang, M. Zhao, J. Fang, et al., ACS Appl. Mater. Interfaces 13 (2021) 12857–12865.
[30] L. Cheng, W. He, H. Gong, et al., Adv. Funct. Mater. 23 (2013) 5893–5902.
[31] X.D. Zhang, H. Wang, A.L. Antaris, et al., Adv. Mater. 28 (2016) 6872–6879.
[32] T.B. Ren, Z.Y. Wang, Z. Xiang, et al., Angew. Chem. Int. Ed. 60 (2021) 800–805.
[33] B. Li, L. Lu, M. Zhao, et al., Angew. Chem. Int. Ed. 57 (2018) 7483–7487.
[34] Q. Wen, Y. Zhang, C. Li, et al., Angew. Chem. Int. Ed. 58 (2019) 11001–11006.
[35] Z. Feng, S. Bai, J. Qi, et al., Adv. Mater. 33 (2021) 2008123.
[36] W. Zeng, X. Wu, T. Chen, et al., Adv. Funct. Mater. 31 (2021) 2008362.
[37] J. Huang, K. Pu, Chem. Sci. 12 (2020) 3379–3392.
[38] C. Bhandari, M. Guirguis, N.A. Savan, et al., Nano Today 36 (2021) 101052.
[39] M. Zhao, J. Ding, Q. Mao, et al., Nanoscale 12 (2020) 6953–6958.
[40] J. Li, C. Liu, Y. Hu, et al., Theranostics 10 (2020) 166–178.
[41] C. Xue, M. Li, C. Liu, et al., Angew. Chem. Int. Ed. 60 (2021) 8938–8947.
[42] S. Wang, B. Li, F. Zhang, ACS Cent. Sci. 6 (2020) 1302–1316.